World Journal of Advanced Research and Reviews
eISSN: 2581-9615 CODEN (USA): WJARAI
Cross Ref DOI: 10.30574/wjarr
Journal homepage: https://wjarr.com/

(RESEARCH ARTICLE)

Check for updates

# Validation of numerical method for the measurement residual stress in low carbon steel weldment

Mercy Kahywuani Madaki [1, †], Reuben Zakari Kabantiyok [2, †, *] and Emmanuel Tanko Dauda [3]

[1] *National Agency for Science and Engineering Infrastructure, Idu Industrial Area Abuja, Nigeria.*
[2] *Defence Industries Corporation of Nigeria, Research and Development Centre, Kakuri, Kaduna, Nigeria.*
[3] *Department of Metallurgical and Materials Engineering, Ahmadu Bello University, Zaria, Nigeria.*
[†] *These authors contributed equally to this work.*

World Journal of Advanced Research and Reviews, 2019, 03(03), 128-142

Publication history: Received on 13 September 2019; Revised 25 october 2019; accepted on 29 october 2019

Article DOI: https://doi.org/10.30574/wjarr.2019.3.3.0140

## Abstract

Residual stress distributions in the longitudinal and transverse directions on a 10mm thick arc welded mild steel plate was determined by using both experimental and numerical methods. Stress measurements were carried out using X-ray diffractometer and finite element method. Welding simulation procedure was developed using the FE-software ANSYS in order to predict residual stresses. ANSYS 12.0 software was used to model the geometry and simulation carried out to verify the results of the XRD. The results obtained showed that as the welding distance increased, the temperature difference between the experimental and finite element analysis (FEA) increased. It was also observed that sample type and welding direction played a vital role in this research. As the welding speed increased, the induced residual stress decreased because less heat was absorbed by the base material and decreased residence time of the arc. Higher Von Mises stress was also observed in the fusion zone and heat affected zone region which experienced plastic deformation. The FEM residual stress predictions show good agreement with the residual stress obtained from XRD analysis.

**Keywords:** Residual stress; Welding; Finite element methods; FEM

## 1. Introduction

Welding remains one of the most versatile and widely used methods for joining metals since its industrial adoption in the 1930s. Its applicability across critical sectors—including shipbuilding, civil infrastructure, aerospace, nuclear energy, and oil and gas pipelines—underscores its pivotal role in modern engineering. [12] [1] [10]. The process offers significant advantages such as high joint strength, excellent structural integrity, and efficient sealing capabilities. However, welding also introduces a series of inherent challenges, chief among them being the formation of residual stresses due to localized heating and subsequent rapid cooling.

Residual stresses are self-equilibrated stresses that remain locked within a component even after the removal of external loads. These stresses arise from the complex interplay of thermal gradients, phase transformations, and differential contraction across the weld zone. While compressive residual stresses may enhance fatigue resistance and retard crack propagation, tensile residual stresses, particularly near weld toes and heat-affected zones (HAZ), can precipitate brittle fracture, fatigue crack growth, and stress corrosion cracking [2] [10] [14].

In welded structures, residual stress magnitudes can reach the material's yield strength, leading to distortion, buckling, and catastrophic failure under service conditions. Residual stresses develop due to varying heating and cooling rate in

* Corresponding author: Reuben Zakari Kabantiyok

different zones near the weld. Different temperature conditions lead to varying strength and volumetric changes in base metal during welding. The variation in temperature and residual stresses owing to movement of heat source along the centerline of weldment is schematically shown in Figure 1.

As heat source comes close to the point of interest, its temperature increases. Increase in temperature decreases the yield strength of a material and simultaneously tends to cause thermal expansion of the metal being heated. However, surrounding low temperature base metal restricts any thermal expansion which in turn develops compressive strain in the metal during heating. Compressive strain initially increases non-linearly with increase in temperature due to variation in yield strength and expansion coefficient of metal with temperature rise. Further, increase in temperature softens the metal, therefore, compressive strain reduces gradually and eventually it vanishes. As the heat source crosses the point of interest and starts moving away from the point of interest, temperature begins to decrease gradually.[7]

The complexity of residual stress development is exacerbated by the multi-physics nature of the welding process. Mechanisms contributing to stress formation include non-uniform thermal expansion, rapid cooling-induced contraction, and phase changes such as austenite-to-martensite transformation during solid-state transitions. [11] These residual stresses manifest in both longitudinal and transverse directions, with high tensile zones often localized along the weld seam and compressive zones forming adjacently within the HAZ.

Given these challenges, modeling and predicting residual stresses have become essential in the design and assessment of welded joints. While experimental techniques such as X-ray diffraction, neutron diffraction, ultrasonic inspection, and hole-drilling provide valuable insights, they are often costly, time-consuming, and limited in spatial resolution or depth penetration. [11]

Non-destructive methods such as the $Sin^2\psi$ X-ray technique allow surface-level stress evaluation with reasonable accuracy and are widely used for calibration and validation [4]. Nevertheless, to complement experimental data and explore stress distribution at scale, numerical modeling—particularly the finite element method (FEM)—has emerged as a powerful alternative.

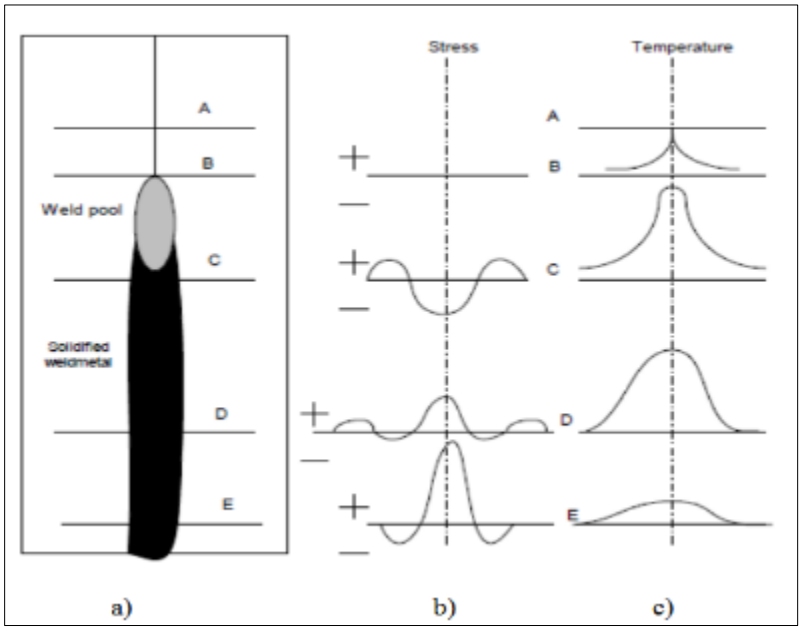


**Figure 1** Schematic diagram showing (a) plate being welded, (b) stress variation across the weld centerline at different locations and (c) temperature of different locations [7]

Recent advancements in computational tools such as ANSYS, ABAQUS, and NX/Nastran have enabled thermo-mechanical simulations that accurately capture weld thermal cycles, material plasticity, phase transformations, and resulting stress fields [3]. These tools not only reduce the time and cost associated with experimental approaches but also allow parametric analysis of welding conditions and materials. Researchers [9] [13] demonstrated the predictive capabilities of FEM in estimating stress evolution in various joint configurations.

This study focuses on the modeling of residual stresses in single V-butt weldments of low carbon steel using ANSYS Multiphysics. Through a combination of experimental analysis and finite element simulations, this research aims to quantify the thermal and mechanical responses induced by shielded metal arc welding (SMAW), validate the models with X-ray diffraction measurements, and provide insights into residual stress mitigation for structural applications. Ultimately, the work contributes to the growing body of literature that advocates for simulation-driven welding process optimization—critical for enhancing the integrity and performance of steel structures in demanding engineering environments.

## 2. Material and methods

### 2.1. Sample Preparation

Low carbon steel plates obtained from the Defense Industries Corporation of Nigeria were cut to 70mm × 100mm × 10mm dimensions (Figure 2). A single V-butt joint configuration was prepared by beveling one of the 70mm edges at a 30° angle, yielding a 60° included angle when two plates were joined. A root gap of 2mm and depth of 2mm was maintained. The samples were austenitized at 920°C for 70 minutes prior to welding to homogenize the microstructure. The electrode selected for welding operations was AWS E6013 with a diameter of 3.2mm.

Welding was conducted using SMAW at 100A and 20V. The electrode was manipulated in a weaving pattern to effectively fuse both sides of the groove. The average welding speed was calculated from the travel distance and time of the electrode, measured using a stopwatch. The plates were rigidly clamped to prevent distortion. Thermocouples were affixed to the surface of the plate to monitor the thermal profiles. A second weld pass was applied after the slag was removed with a wire brush. Proper alignment and fixation were ensured throughout the process. The welds progressed from left to right with consistent torch motion to maintain arc stability and uniform heat input.

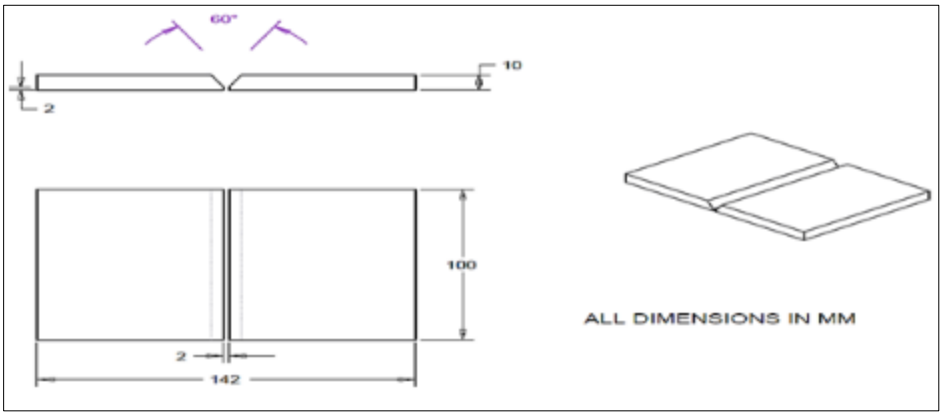


**Figure 2** Geometry for Single-V butt specimen for low carbon steel plates

### 2.2. Chemical Analysis

The chemical composition of the test samples was determined using Optical Emission Spectroscopy (OES). The samples were first prepared as metallographic samples. Then a spark of X-ray was passed through it to disperse different elements present in their respective wavelengths. Any element present in the sample will get excited when its excitation frequency is reached and will be registered.

### 2.3. Residual Stress Measurement

Residual stress was evaluated using the $Sin^2\psi$ method with a Shimadzu XRD 6000diffractometer. Surface stress measurements were performed at seven tilt angles: $0^o$, $10^o$, $20^o$, $30^o$, $40^o$, $50^o$, and $60^o$. For each $\psi$ angle, the diffraction peak position was recorded, allowing computation of the interplanar spacings ($d_\psi$).

The elastic strain at each angle was calculated using, $\varepsilon_\psi = (d_\psi - d_0) / d_0$

where:

- $d_\psi$ is the interplanar spacing at tilt angle $\psi$

- $d_0$ is the stress-free lattice spacing

A linear regression of $d_\psi$ versus $\sin^2\psi$ was performed, and the slope (m) of the resulting line was used to compute the residual stress ($\sigma$) using the following equation: $\sigma_\varphi = m / d_0 . E / (1 + \nu)$

where:

- E is the Young's modulus of the material
- $\nu$ is the Poisson's ratio

This method enabled accurate surface-level residual stress quantification and provided a reliable basis for comparison with finite element analysis (FEA) predictions. The nondestructive nature and proven surface sensitivity of XRD make it especially suitable for analyzing residual stress fields in welded metallic components.

### 2.4. FEA Modeling Procedure

Residual stress modeling from Shielded Metal Arc Welding (SMAW) was performed using ANSYS Workbench by coupling transient thermal and structural analysis systems. The weld geometry, a single V-butt joint (Figure 2), was modeled in DesignModeler and meshed (Figure 3) with 3806 nodes and 2038 triangular elements. Temperature-dependent material properties were assigned, and boundary conditions were applied to replicate actual welding constraints.

A moving heat source was modeled through a transient heat input, with time steps set to 1 second to control the electrode speed. The Newton–Raphson solver (NROPT, FULL) was activated to handle nonlinearity and element activation. Heat input based on welding parameters was applied through reference temperature settings.

The results of the thermal analysis were transferred to the structural module, where the temperature acted as body loads. A fixed boundary condition was imposed on the bottom surface to simulate clamping. The structural analysis yielded residual stress distributions, which were compared with XRD measurements for validation.

## 3. Results and Discussions

### 3.1. Chemical Analyses of the Test Samples

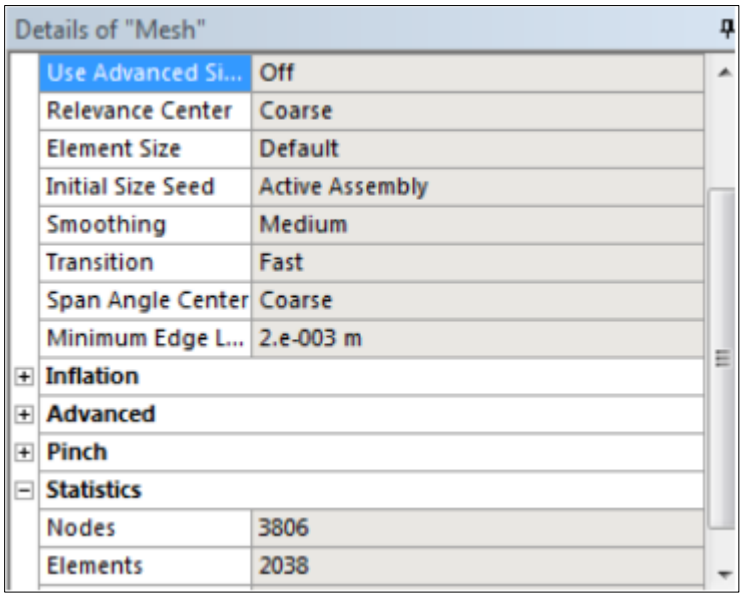


**Figure 3** Meshed details

The chemical compositions of the low carbon steel specimens used in this study were determined through spectrometric analysis and are presented in Tables 1. The main alloying elements identified include carbon (C), manganese (Mn), silicon (Si), phosphorus (P), sulfur (S), chromium (Cr), nickel (Ni), molybdenum (Mo), tungsten (W),

copper (Cu), aluminum (Al), and iron (Fe). Specimens A, B, and C fall within the typical composition range for low carbon steels, with Fe as the base element and trace additions of other elements to improve strength, toughness, and weldability.

### 3.2. Thermal Analysis

The thermal response during welding was modeled using transient thermal analysis, simulating the passage of a moving heat source across the weld line. The movement of the arc was discretized such that it remained over each finite element node for a defined time increment, enabling sufficient localized heat input before transitioning to adjacent nodes. This approximation is widely adopted in welding simulations and has shown good accuracy in capturing peak thermal gradients. [5]

**Table 1** Chemical Composition of Low Carbon Steel Specimens A, B, and C

| **Elements** | **C** | **Si** | **Mn** | **P** | **Cu** | **Al** | **S** | **Cr** | **Ni** | **Mo** | **W** | **Fe** |
|---|---|---|---|---|---|---|---|---|---|---|---|---|
| Specimen A | 0.0500 | 0.1530 | 0.6300 | 0.0600 | 0.0400 | 0.0300 | 0.0100 | 0.0100 | 0.0200 | 0.0100 | 0.0880 | Balance |
| Specimen B | 0.0638 | 0.1530 | 0.5829 | 0.0804 | 0.0402 | 0.0400 | 0.0416 | 0.0184 | 0.1067 | 0.0752 | 0.0886 | Balance |
| Specimen C | 0.0975 | 0.0145 | 1.3470 | 0.0777 | 0.0975 | 0.0050 | 0.0406 | 0.0399 | 0.0946 | 0.1112 | 0.1590 | Balance |

Temperature distributions were obtained at selected nodes on the plate throughout the welding process. Figures 4a, b, and c show the temperature contours for samples A, B, and C, respectively. The peak temperatures recorded were 1668.5°C for Sample A, 1711.8°C for Sample B, and 1690.1°C for Sample C. These values are consistent with the arc temperature measured via K-type thermocouples, which was approximately 1800°C. Notably, the contour plots revealed a clear thermal gradient with temperature decreasing as the distance from the weld center increased, validating expected heat dissipation patterns in arc welding. [15]

The initial ambient and base metal temperature was set to 25°C. Heat input values of 800 J/mm, 666.67 J/mm, and 500 J/mm were used for Samples A, B, and C, respectively. Sample A received the highest heat input, resulting in the largest fusion zone and heat- affected region. Finer mesh densities were employed near the weld line to better capture steep thermal gradients and improve computational accuracy.

A comparative evaluation of experimental and finite element temperature distributions is presented in Table 2. As the measurement distance, d(mm) from the weld center increased, discrepancies between experimental and simulated temperatures also increased. For instance, a temperature deviation of 3.44% was observed at 10 mm from the weld line, increasing to 6.20% at 30 mm. These differences are within acceptable engineering limits and align with previously reported validation studies of welding thermal models.[9]

The observed trend—that higher temperatures are recorded at points nearer the weld center—is consistent with the inverse-square law of heat dissipation and further substantiates the fidelity of the FEM approach. The close agreement between experimental results and finite element simulations confirms the validity of the adopted thermal model, which is suitable for subsequent stress analysis coupling. This comparative study reaffirms the robustness of the thermal model in simulating arc welding processes, in line with contemporary works on weld simulation fidelity.

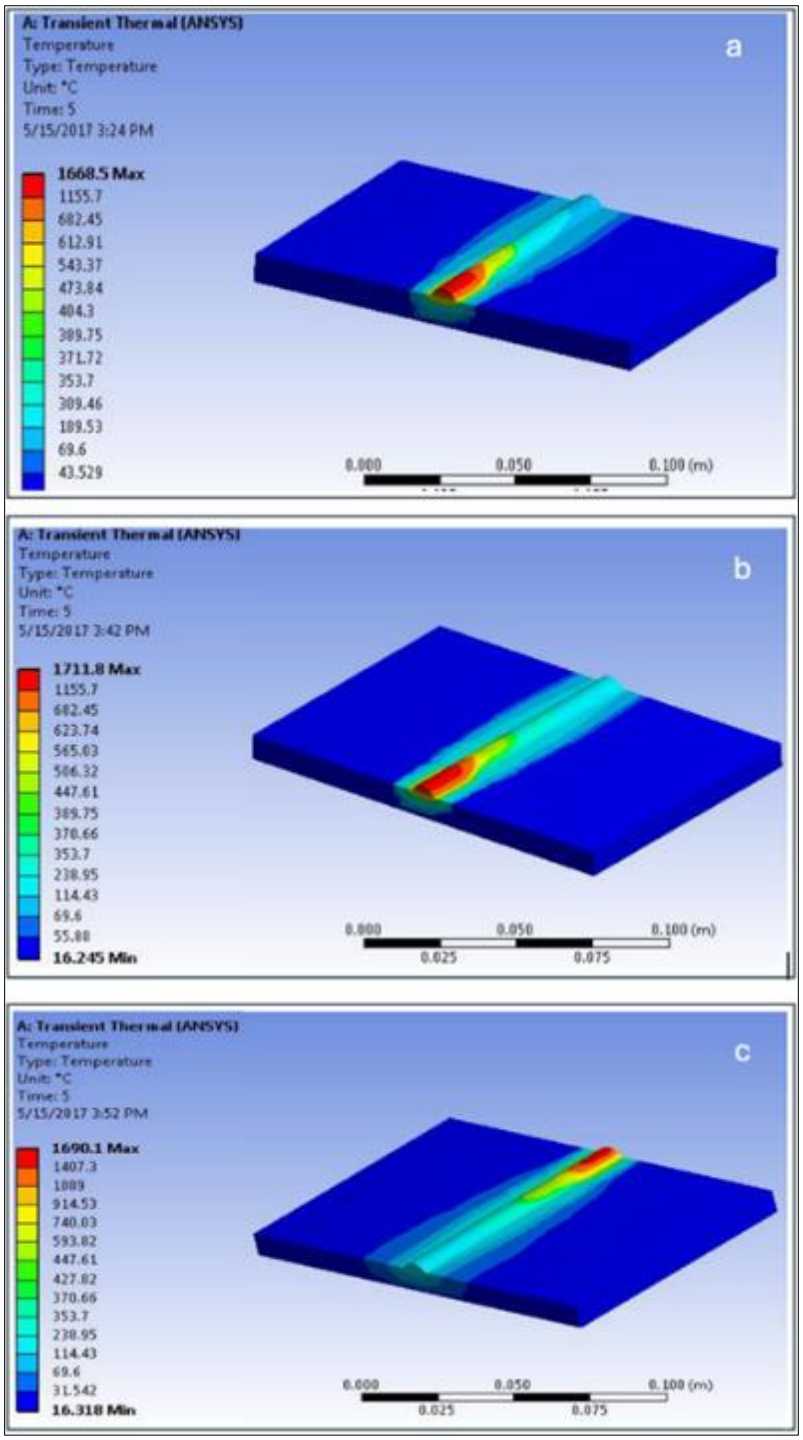


**Figure 4** Temperature distribution for specimen: (a) A, (b) B, (c) C

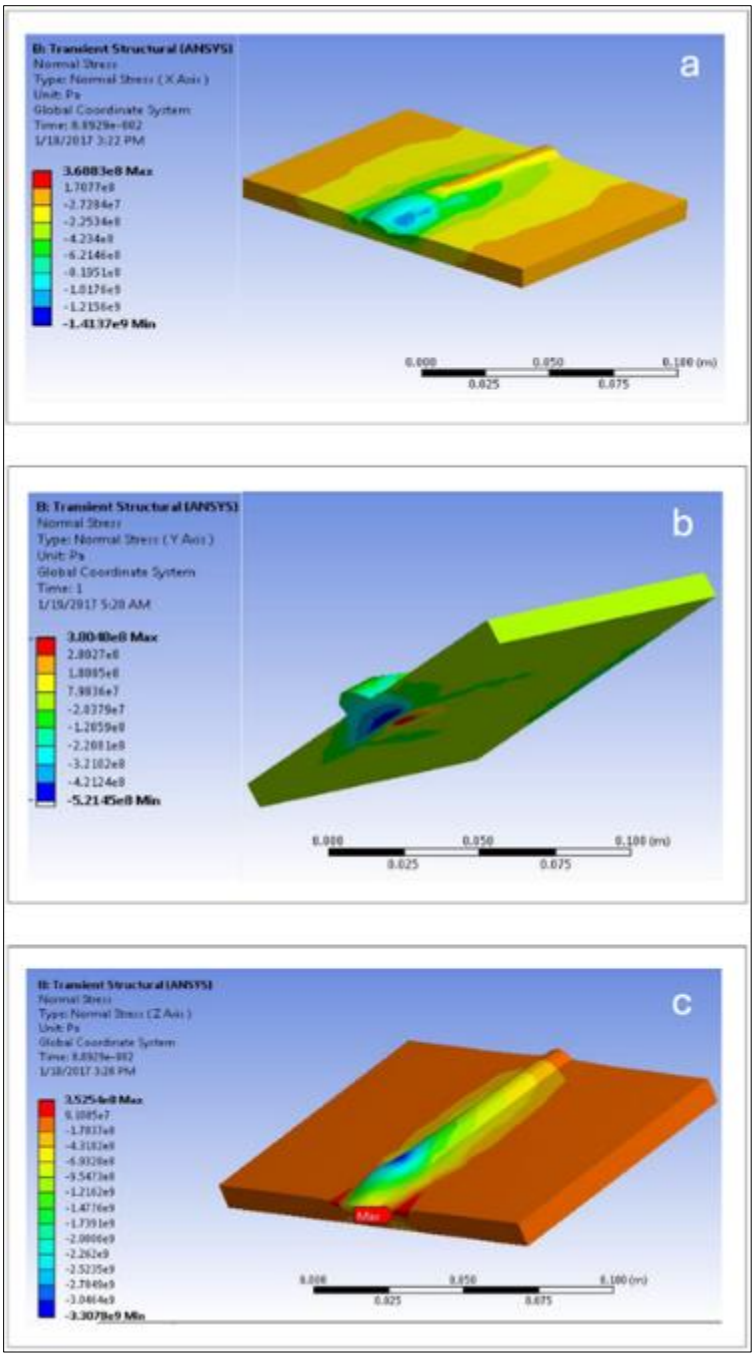


**Figure 5** Normal Stress for sample A: (a) x-axis, (b) y-axis, (c) z-axis

The validated model provides a sound basis for coupling with mechanical analysis to predict residual stress distributions.

**Table 2** Comparison of Experimental and FEA Temperature Distribution

| d (mm) | Temp by Exp (°C) | Temp by FEA (°C) | % difference |
|---|---|---|---|
| 10 | 600.4 | 580.4 | 3.44 |
| 20 | 310.5 | 298.2 | 4.12 |
| 30 | 202 | 110.2 | 6.20 |

### 3.3. Stress Analysis

The stress analysis of the welded samples was carried out using finite element modeling, and the resulting stress distributions were evaluated in all three orthogonal directions. Figures 5a, b, and c display normal stress contours in the X, Y, and Z directions for sample A. The stress values exhibited a smooth gradient transition from high tensile to compressive regions, particularly within the fusion and heat-affected zones (HAZ). Maximum stresses approached critical levels near the weld line but remained below the yield strength of the material (390 MPa), suggesting safe stress distribution under the given thermal conditions.

X-ray diffraction (XRD) measurements for Sample A, presented in Table 3 indicated surface stress values ranging from 20.73 MPa to 352 MPa in the X-direction. The FEM-predicted values (Table 4) in the same direction ranged from -14.1 MPa to 368 MPa. In the Y-direction, XRD values ranged from -255 MPa to 377 MPa, while FEM results showed a span of -521 MPa to 380 MPa. The Z-direction stress from XRD was found to be between -30.1 MPa and 340 MPa, with FEM predictions from -33.1 MPa to 352.54 MPa. The reasonably close correlation between experimental and simulated data confirms the fidelity of the stress model.

**Table 3** Residual stresses obtained using XRD for the three test samples

| Direction | Sample A (MPa) | Sample B (MPa) | Sample C (MPa) |
|---|---|---|---|
| X | 352 to 20.73 | 124 to -260 | 136 to - 44.50 |
| Y | 377 to -2551 | 162 to -182 | 370 to -435.3 |
| Z | 340 to -30.10 | 330 - 26.00 | 120 to -15.00 |

**Table 4** Residual obtained from FEA modeling for the three test samples

| Direction | Sample A (MPa) | Sample B (MPa) | Sample C (MPa) |
|---|---|---|---|
| X | 368 to -14.1 | 135 to -526 | 139 to -54.05 |
| Y | 380 to -521 | 163 to -173 | 344.02 to-454.8 |
| Z | 352.54 to -33.1 | 352 to -33.07 | 120 to -15.00 |
| Eq Stress | 426 | 376.6 | 347.65 |

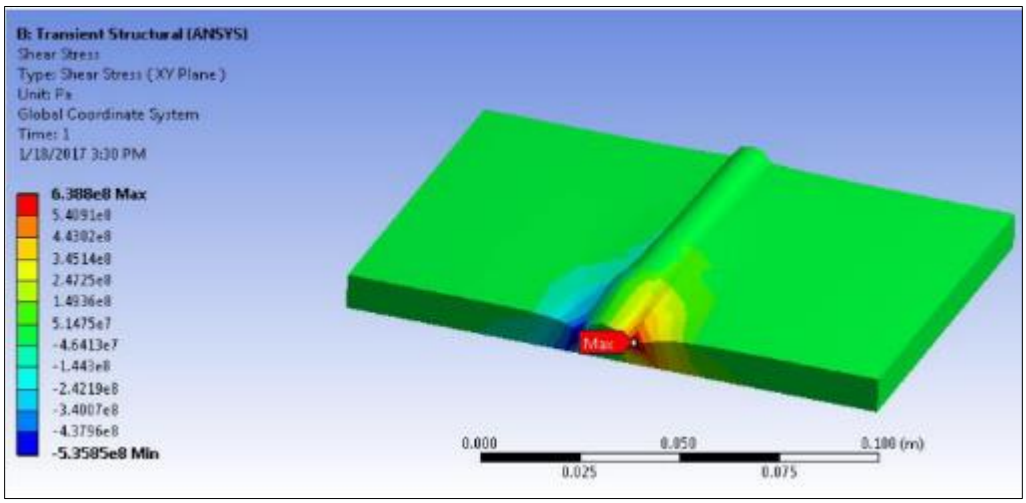


**Figure 6 S**hear stress distribution for sample A

Figure 6 presents the shear stress distribution, with peak shear stresses reaching approximately 600 MPa. Based on the stress contours, shear onset was observed around 400 MPa, indicating potential initiation of plastic deformation under critical conditions.

The Von Mises stress analysis provides insight into the structural integrity of the welded samples under service conditions. For Sample A, the maximum Von Mises stress was observed to be 405 MPa (Figure 7a), which exceeds the material's yield strength of 390 MPa. This indicates the presence of localized yielding, suggesting that while most of the structure remains within the elastic regime, certain zones may experience plastic deformation under operational loading. In contrast, Sample B exhibited a peak Von Mises stress of 376 MPa (Figure 7b), which remains marginally below the yield strength threshold. This implies that Sample B is less likely to experience plastic deformation and is expected to retain its structural integrity during service. Sample C demonstrated the most conservative stress response, with a maximum Von Mises stress of 347 MPa (Figure 7c). This value is well within the yield limit of the material (370 MPa), indicating that the welded structure of Sample C is likely to perform reliably under typical loading conditions without permanent deformation.

For Sample B, Figures 8 illustrate transient stress distributions. The stress ranges remained well within the yield strength of 390 MPa. XRD-measured stresses in the X-direction were from -260 MPa to 124 MPa, while FEM values ranged from -526 MPa to 135 MPa. In the Y-direction, XRD ranged from -182 MPa to 162 MPa, while FEM reported -173 MPa to 163 MPa. For the Z-direction, XRD and FEM values were -26 MPa to 330 MPa and -33.07 MPa to 352.54 MPa respectively. These close ranges indicate a fair match and support the reliability of the model. Figures 9 show the stress profiles for Sample C. Both compressive and tensile stresses were observed, with all normal stress values remaining below the yield strength of 370 MPa.

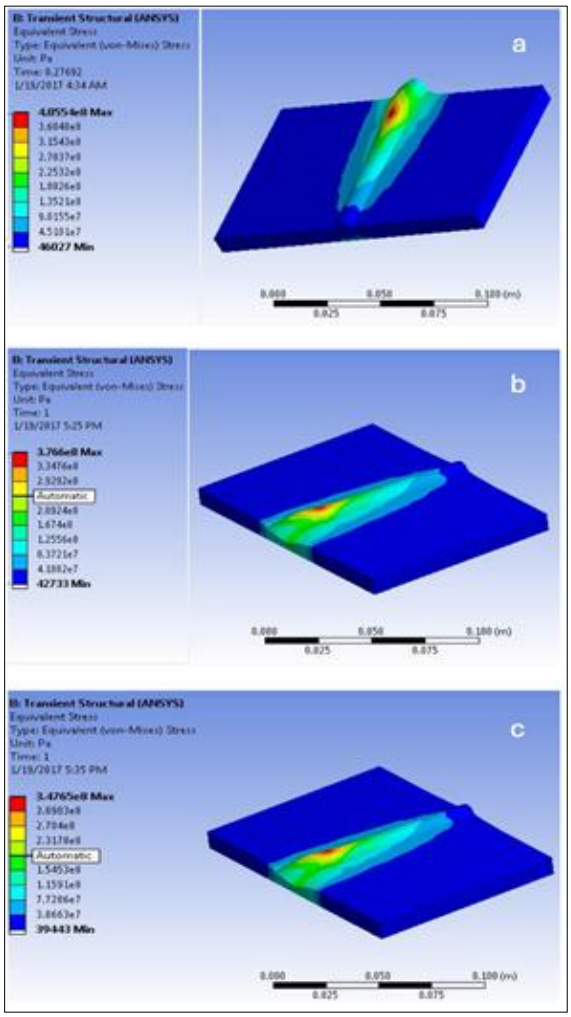


**Figure 7** Von mises stress for distributions sample A, B, C

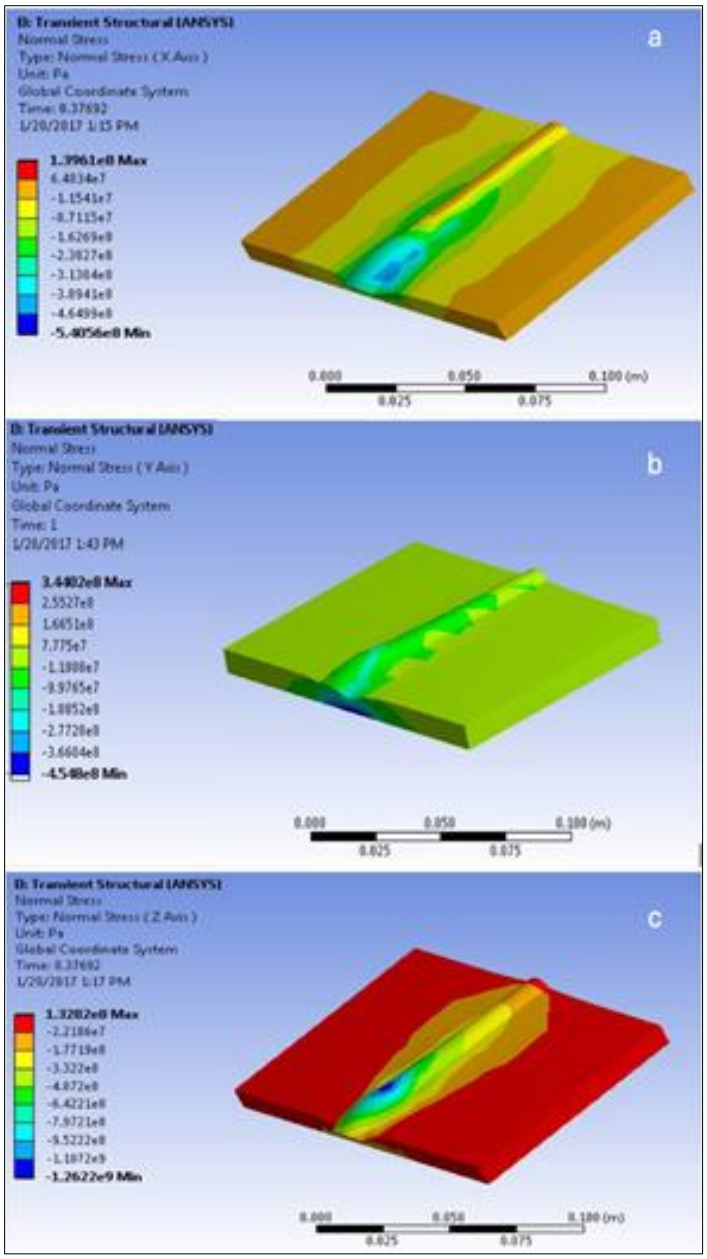


**Figure 8** Normal Stress for sample B: (a) x-axis, (b) y-axis, (c) z-axis

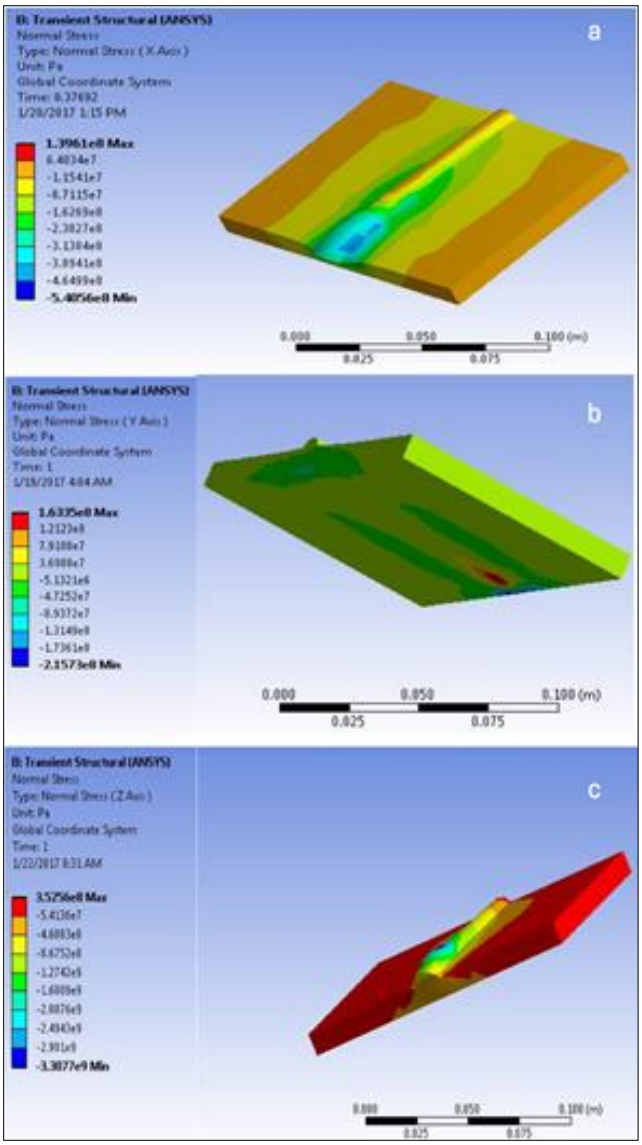


**Figure 9** Normal Stress for sample C: (a) x-axis, (b) y-axis, (c) z-axis

These findings highlight the influence of welding parameters and material properties on the stress response of welded joints, reinforcing the utility of finite element simulations in predicting failure-prone zones and optimizing weld design. The results are consistent with empirical findings in the literature, which indicate that FEM models, when appropriately calibrated with XRD data, provide robust predictions of residual stress distributions in welded structures. The close agreement between experimental and simulated values validates the modeling approach and confirms the suitability of the FE method for predicting welding-induced stress states.

### 3.4. Residual Stress Analysis

Residual stresses generated during welding were assessed both experimentally using X-ray diffraction (XRD) and numerically through finite element modeling in ANSYS Multiphysics. The measurements were focused along three principal axes: longitudinal (parallel to the weld bead), transverse (perpendicular to the weld), and normal (through the thickness of the material). The data captured both tensile (positive) and compressive (negative) stress regions, providing a full picture of the post-weld stress state.

Notably, tensile and compressive stresses were distributed in a way that preserved overall mechanical balance. While longitudinal and transverse directions carried the majority of the residual stress load, through-thickness stresses were prominent only near the weld ends and diminished away from these regions.

The type of steel sample and the welding direction significantly influenced the magnitude and distribution of residual stress. For example, the highest tensile stresses were recorded in the Y-direction for Samples A and C, whereas Sample B showed its maximum tensile stress in the Z-direction. Minimum compressive stress followed a similar but inverse trend—occurring in the Y-direction for Samples A and C and in the X-direction for Sample B.

Comparisons between the XRD results and FEM predictions showed strong agreement, especially in the transverse direction. For instance, residual stress in Sample A measured via XRD ranged from 352 MPa (tensile) to -20.73 MPa (compressive), while FEM predicted a range from 368 MPa to -14.1 MPa. This consistency strengthens confidence in the FEM model and highlights its usefulness in evaluating welded structures.

Stress distribution patterns, as illustrated in Figures 10, further reinforce this alignment, particularly for Sample A. Samples B and C showed comparatively lower residual stresses, likely due to higher welding speeds. This correlation aligns with established findings that increasing welding speed reduces the heat input per unit length, thereby limiting residual stress formation.[8]

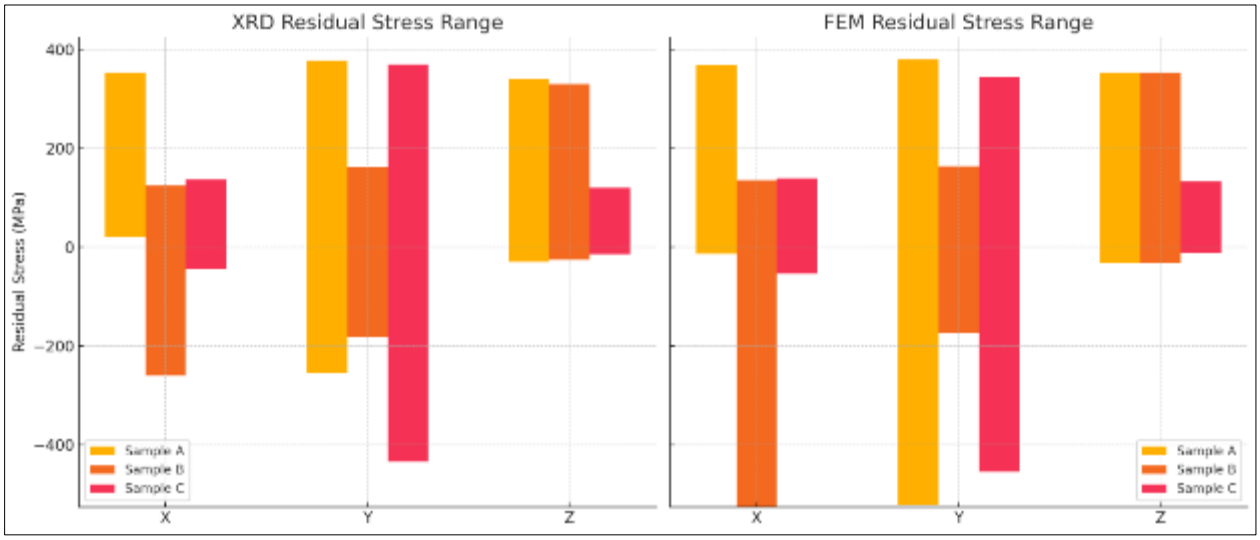


**Figure 10** Residual stress induced in the materials for experimental and FEM

To validate these findings, statistical comparisons using the P-test were conducted. Sample A showed the strongest correlation between experimental and simulated results, affirming the reliability of FEM for this application. In general, the results demonstrate that finite element modeling, when properly calibrated, can serve as a predictive tool to manage residual stress in welded components, reducing the need for extensive experimental trials.

### 3.5. Sustainable Materials Perspective in Welded Structures

Recent trends in materials engineering have placed a strong emphasis on the development and integration of sustainable materials within structural applications. Among these, Natural Fibre Reinforced Polymer Composites (NFRPCs) have garnered significant interest as viable alternatives to conventional glass and carbon fibre composites. These bio-based materials offer high specific strength-to-weight ratios, are cost-effective, environmentally friendly, and exhibit good recyclability—all desirable characteristics for modern engineering structures. [6]

Although their adoption in high-temperature processes such as fusion welding remains limited due to thermal sensitivity, their relevance is increasing in hybrid assemblies where mechanical fastening or low-heat joining methods (e.g., friction stir welding, adhesive bonding) are employed. Moreover, the advancement of finite element modeling (FEM) in welding research, including stress and thermal simulations as presented in this study, can be extended to investigate thermal gradients and residual stress fields in composite-to-metal interfaces.

Researchers have emphasized that leveraging locally available natural fibres could provide pathways toward energy-efficient fabrication without compromising mechanical integrity.[6] As sustainable engineering evolves, integrating residual stress control and predictive modeling into the design and joining of such eco-conscious composites will be critical in expanding their application into thermomechanical systems.

### 3.6. Statistical Analysis of Residual Stress Correlation

To quantify the agreement between experimental (XRD) and numerical (FEM) measurements of residual stresses, a statistical P-test was performed. The P-test in this context represents the Pearson correlation coefficient, assessing the linear correlation between residual stress values obtained from both methods across different spatial directions (X, Y, Z).

For each sample, the XRD and FEM residual stress values were paired and analyzed. A P-value (correlation coefficient) close to 1.0 indicates a strong positive linear correlation, implying that the FEM model effectively replicates the experimentally observed stress behavior. Conversely, a lower P-value indicates divergence between the predicted and measured stress values. As shown in Table 5, Sample A yielded a high correlation coefficient (P = 0.961), demonstrating excellent agreement in maximum tensile stress values across all directions. This suggests that the FEM model for Sample A is highly reliable and accurately captures the thermomechanical effects of welding.

**Table 5** P-test Results for Maximum Tensile Residual Stresses (XRD vs FEM)

| Sample | XRD (MPa) | | | FEM (MPa) | | | P-test |
|---|---|---|---|---|---|---|---|
| | X | Y | Z | X | Y | Z | |
| A | 352 | 377 | 340 | 368 | 380 | 352.54 | 0.961 |
| B | 124 | 162 | 135 | 135 | 163 | 352 | - |
| C | 136 | 370 | 139 | 139 | 344.02 | 132 | - |

**Table 6** P-test Results for Minimum Compressive Residual Stresses (XRD vs FEM)

| Sample | XRD (MPa) | | | FEM (MPa) | | | P-test |
|---|---|---|---|---|---|---|---|
| | X | Y | Z | X | Y | Z | |
| A | 20.73 | -255 - | -30.1 | -14.1 | -521 | -33.1 | - |
| B | -260 | 30.1 | -26 | -526 | -173 | -33.07 | 0.808 |
| C | -44.5 | -435.3 | -15 | -54.05 | -454.8 | -12.62 | 0.708 |

In Table 6, Sample B and C showed moderate correlation for compressive stresses (P = 0.808 and P = 0.708 respectively), which is still within acceptable engineering tolerance. The slightly reduced correlation may be attributed to differences in local microstructural evolution or mesh sensitivity in the FEM model, particularly in regions of steep stress gradients.

These results reinforce the validity of the FEM modeling approach, especially for samples with well-characterized thermal input and boundary conditions. Moreover, they confirm the utility of XRD validation in improving model accuracy for weld-induced residual stress prediction

## 4. Conclusion

This study investigated the modeling of residual stresses in single V-butt weldments of low carbon steel using coupled thermo-mechanical analysis in ANSYS Multiphysics. Three distinct compositions of low carbon steel plates were successfully fabricated and welded using Shielded Metal Arc Welding (SMAW). The welding process was effectively simulated using the Finite Element Method (FEM), with residual stress distributions arising from localized thermal cycles being computed and visualized.

Experimental validation was performed using X-ray diffraction, and a strong correlation was observed between FEM predictions and measured residual stress values. This agreement affirms the accuracy of the FEM-based simulation framework and its applicability in predictive modeling for welded structures. The results demonstrate that FEM can serve as a reliable pre-weld analysis tool for optimizing process parameters and minimizing deleterious stress concentrations in critical structural components.

To further enhance the understanding and application of residual stress modeling in welded structures, the following recommendations are proposed:

- Mechanical Property Assessment: Future studies should include fatigue, creep, and fracture toughness tests to evaluate the long-term performance and durability of the weldments under service conditions.
- Microstructural Characterization: High-resolution imaging techniques such as Scanning Electron Microscopy (SEM) and Electron Backscatter Diffraction (EBSD) are recommended to investigate the weldment interface and the evolution of microstructural features contributing to stress development.
- Material and Process Variants: Further investigations should incorporate different steel grades, welding methods, and post-weld heat treatments to establish a broader database for predictive modeling using FEM.
- 3D Simulation Enhancement: Extending the simulations to full 3D models with more refined meshing and adaptive heat source modeling could improve accuracy in capturing complex geometrical and thermal behaviors during welding.

These future directions will not only validate the robustness of numerical approaches but also inform the development of optimized welding procedures tailored for safety- critical applications in aerospace, construction, and power generation industries.

## Compliance with ethical standards

*Disclosure of conflict of interest*

No conflict of interest to be disclosed.

## References

[1] Mohammad Alam. Structural integrity and fatigue crack propagation life assessment of welded and weld-Repaired structures. Doctor of Philosophy, Louisiana State University and Agricultural and Mechanical College, October 2005.

[2] Mohammed Belassel. Residual Stress Measurement using X-Ray Diffraction Techniques, Guidelines and Normative Standards. SAE International Journal of Materials and Manufacturing, 5(2):352–356, April 2012.

[3] Peng-Hsiang Chang and Tso-Liang Teng. Numerical and experimental investigations on the residual stresses of the butt-welded joints. Computational Materials Science, 29(4):511–522, April 2004.

[4] Michael E Fitzpatrick, Antony Thomas Fry, Philip Holdway, FA Kandil, J Shackleton, and L Suominen. Determination of residual stresses by x-ray diffraction. 2005.

[5] John Goldak, Aditya Chakravarti, and Malcolm Bibby. A new finite element model for welding heat sources. Metallurgical transactions B, 15:299–305, 1984.

[6] Reuben Kabantiyok, DS Yawa, and MO Afolayan. Application of taguchi approach in the optimization of the mechanical properties of snail-shell-filler/chicken-feather-fibre polymer based hybrid composite. European Journal of Engineering Science and Technology, 1(1):39–54, 2018.

[7] Sindo Kou. Welding metallurgy.NewJersey,USA, 431(446):223–225, 2003.

[8] Sushil Kumar Maurya and AK Jain. Experimental and finite element analysis of single-v groove butt weld on weld pool geometry of aluminium alloy plate under different joint parameter. International Journal for Scientific Research and Development, 3:639–644, 2015.

[9] N. Murugan and R. Narayanan. Finite element simulation of residual stresses and their measurement by contour method. Materials and Design, 30(6):2067–2071, June 2009.

[10] RS Parmar. Welding engineering and technology. Khanna publishers, 2010.

[11] N.S. Rossini, M. Dassisti, K.Y. Benyounis, and A.G. Olabi. Methods of measuring residual stresses in components. Materials and Design, 35:572–588, March 2012.

[12] SM Rozza. Automatic welding table. Bachelor thesis, material science and engineering, Faculty German university in Cairo, 2012.

[13] Dragi Stamenković and Ivana Vasović. Finite Element Analysis of Residual Stress in Butt Welding Two Similar Plates.

[14] Tso-Liang Teng, Chin-Ping Fung, Peng-Hsiang Chang, and Wei-Chun Yang. Analysis of residual stresses and distortions in T-joint ®llet welds.

[15] S.A. Tsirkas. Numerical simulation of the laser welding process for the prediction of temperature distribution on welded aluminium aircraft components. Optics and Laser Technology, 100:45–56, March 2018.